Effect of a Plasticizer on the Structure of Biodegradable Starch/Clay Nanocomposites: Thermal, Water-Sorption, and Oxygen-Barrier Properties

C. Zeppa, F. Gouanvé, E. Espuche

Ingénierie des Matériaux Polymères, Unités Mixtes de Recherche/Centre National de la Recherche Scientifique 5223, Laboratoire des Matériaux Polymères et des Biomatériaux, Bâtiment Institut des Sciences et Techniques de l' Ingénieur de Lyon, 15 Boulevard André Latarjet, Université Claude Bernard Lyon 1, 69622 Villeurbanne Cedex, France

Received 26 June 2008; accepted 24 September 2008
DOI 10.1002/app.29588
Published online 13 February 2009 in Wiley InterScience (www.interscience.wiley.com).

ABSTRACT: In this study, we investigated nanocomposites based on a plasticized natural biodegradable matrix. The polymer used was a natural potato starch, and the plasticizers were glycerol and a urea/ethanolamine mixture. A natural and an organically modified montmorillonite were studied. Two series of films containing 6 wt % nanoclays were prepared by a solution/cast process: the first series was based on neat starch, and the second one was based on 20 wt % plasticized starch. For all matrices, a mixture of intercalated and exfoliated structures was formed by the addition of pristine montmorillonite, whereas an aggregate structure was obtained with organoclay. The thermal stability was not significantly influenced by the addition of clays. Water sorption was examined as a function of the matrix and clay hydrophilicity. The significant reduction of oxygen permeability obtained with natural montmorillonite was related to the high dispersion state of this clay. For urea–ethanolamine composites, specific compatibilizer/clay interactions led to an improvement again in the barrier properties. © 2009 Wiley Periodicals, Inc. J Appl Polym Sci 112: 2044–2056, 2009

Key words: barrier; biodegradable; clay; gas permeation; nanocomposites

INTRODUCTION

Biodegradable polymers from renewable resources have attracted much attention in recent years.[1–3] Renewable sources of polymeric materials offer an alternative for maintaining the sustainable development of economically and ecologically attractive technologies. Indeed, the complete biological degradability of these polymers can contribute to a reduction in the volume of garbage and the protection of the climate through the reduction of carbon dioxide released. Thus, there is considerable interest in replacing some or even a large amount of synthetic polymers with biodegradable materials in many applications. In the family of renewable-sources-based biodegradable polymeric materials, starch has been considered one of the most promising materials because it is readily available and may form cost-effective end products. Starch is the major form of carbohydrate in plants. It is a semicrystalline polymer composed of a mixture of amylose, an essentially linear polysaccharide, and amylopectin, a highly branched polysaccharide.[4] The relative amount of amylose and amylopectin depends on the plant source.

In packaging applications, starch-based materials have received great attention because of their biodegradability, wide availability, and low cost. Nevertheless, in the absence of plasticizers, films made from starch are very brittle because of extensive intermolecular forces. So, starch is commonly pretreated with a plasticizer to overcome film brittleness and to make enabling processing.[5–7] However, plasticized starch cannot meet all the requirements of packaging applications. In particular, these materials remain water sensitive and, therefore, lose their barrier properties upon hydration.[8–10] In this context, the nanocomposites concept can be a promising option.

Special attention has been paid to clays in the field of nanocomposites because of their small particle size, extremely large surface areas, aspect ratios, and intercalation properties.[11,12] The incorporation of layered silicate in polymers and especially in synthetic polymers has already demonstrated significant enhancements in a large number of physical properties, including barrier properties, flammability resistance, and thermal and environmental stability.[13–19] All of these properties depend to a great part on the clay dispersion state. Improved properties have been usually obtained for exfoliated structures.

Correspondence to: F. Gouanvé (fabrice.gouanve@univ-lyon1.fr) or E. Espuche (eliane.espuche@univ-lyon1.fr).

TABLE I
Characteristics of the Nanoclays

Commercial name	Nanofil 757	Cloisite 30B
Montmorillonite code	MMT-Na^+	MMT-OH
Chemical structure of organic modifiers	—	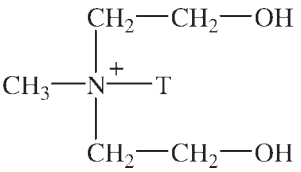
Inorganic content (w/w %)[a]	100	78.9
Cation-exchange capacity	100 mequiv/100 g	90 mequiv/100 g
Specific gravity (g/cm^3)	2.60	1.98
d_{001} (Å)[b]	11.7	18.5

[a] Determined by TGA.
[b] Interplatelet distance determined by XRD analysis.

Furthermore, some studies have also shown that strong interactions between the impermeable fillers and the polymer could benefit the permeability reduction, as the interface between the silicate platelet and the matrix becomes then a low diffusive gas pathway.[20] However, among all the studies concerned with nanocomposites, very few studies have been related to natural polymers and, in particular, with starch or plasticized starch.[9,21,22]

The aim of this study was to prepare environmentally friendly composites from biodegradable starch and nanoclay and to investigate the role played by the presence of a plasticizer in the dispersion of nanoclay and in the final properties. Two plasticizers were chosen: glycerol and a mixture of urea/ethanolamine (50/50). Glycerol is the most common plasticizer used in starch films,[23–25] whereas urea/ethanolamine mixture is an alternative plasticizer, which can form strong interactions with starch.[9,21,22,26] To modify the affinity between the clay and the different matrices, two nanoclays were also used: a natural montmorillonite and an organically modified montmorillonite. The aim of our study was to establish the relationships between the structure, morphology, and transport properties for these different materials. In particular, the state of dispersion of the nanoclays was examined as a function of the filler modification and of the composition of the matrices. The crystalline morphology of the matrices in the nanocomposites was also determined. Indeed, the polymer crystalline phase was considered impermeable to small molecules, and a modification of this phase after the incorporation of the nanoclays could then greatly modify the transport properties. Oxygen permeability coefficients were determined at 50% relative humidity, which is a standard use condition. The permeability evolution was examined as a function of the clay dispersion state but also as a function of the water sorption mechanism for each material. Indeed, water molecules are well known as a plasticizer for starch-based materials and can then also play a significant role in the oxygen permeability.

EXPERIMENTAL

Materials

Native potato starch with a weight ratio of amylopectin to amylose equal to 77 : 23% was purchased from Sigma. Glycerol (+99% purity) was supplied by Aldrich (Steinheim, Germany). Urea and ethanolamine were provided by Prolabo (Paris, France). Two nanoclays were used in this study. Nanofil 757, denoted as MMT-Na^+, was supplied by Süd Chemie (Munich, Germany), and Cloisite 30B, denoted as MMT-OH, was provided by Southern Clay Products (Gonzales, TX). Nanofil 757 is a natural purified montmorillonite with a cation-exchange capacity of 100 mequiv/100 g. Cloisite 30B is a natural montmorillonite modified with methyl tallow bis-2-hydroxyethyl quaternary ammonium and has a cation-exchange capacity of 90 mequiv/100 g. The tallow chains of the surfactant have a composition of about 65% C18, 30% C16, and 5% C14. The main characteristics of the nanoclays are listed in Table I.

Film preparation

Three reference films were prepared for this study. The first one was composed of only starch, and the other two were composed of plasticized starch. Glycerol and a mixture of urea/ethanolamine (50/50 wt %) were used as plasticizers. The weight ratio of starch to plasticizer was fixed at 80/20 in all cases. The film preparation consisted of the dissolution of starch with or without plasticizers in distilled water at a concentration of 3% w/w. The solutions were heated to the gelatinization temperature (85°C) and continuously stirred at this temperature for 1 h. The resulting solutions were poured in polystyrene Petri dishes, and evaporation was carried out at ambient

temperature. Films about 45–55 μm thick were obtained, and they were conditioned at 20°C and 40% relative humidity between two sheets of polyethylene for 10 days before film characterization. The reference films were named S, SG, and SUE for the pure starch film, glycerol-plasticized starch film, and urea/ethanolamine-plasticized starch film, respectively.

For the nanocomposite preparation, a 0.5 wt % dispersion of layered silicate was prepared by the addition of the nanoclays to distilled water. The suspension was stirred for 48 h for MMT-OH and 12 h for MMT-Na^+ with a magnetic stirrer at ambient temperature. Then, the starch solution and clay suspension were mixed. The resulting mixture was heated at 85°C for 5 h under continuous stirring. The process of nanocomposite films formation and storage were similar to that used for the formation of the reference films. For all nanocomposites, the percentage of nanoclays was fixed at around 6 wt %.

X-ray diffraction (XRD)

XRD analyses were carried out with a Cu tube and a Bruker (Champs-sur-Marne, France), D8 Advance diffractometer, where the Kβ line was removed with a nickel filter. The diffraction patterns were obtained at room temperature in the range of 2θ between 1 and 30° by steps of 0.02°. The films were deposited on neutral monosubstrates with a thin transfer adhesive with a low scattering response. The analyses were performed after conditioning the films 10 days at 20°C and 40% relative humidity.

Transmission electron microscopy (TEM)

For TEM analysis, samples were microtomed at −120°C with a Leica (Reuil Malmaison, France) EMFCS instrument equipped with a diamond knife to obtain ultrathin sections 70–80 nm thick. The samples were imaged in a Philips (Eindhoven, Netherlands) CM120 transmission electron microscope with an accelerating voltage of 80 kV.

Thermogravimetric analysis (TGA)

TGA was performed with a TGA 2950 (TA Instruments, Guyancourt, France). Data were collected on samples of 5–10 mg during a ramp of temperature from 30 to 500°C at 10°C/min under a dry nitrogen atmosphere. The weight fraction of nanoclays in the composites were determined from the values of the residues obtained at 450°C. The first derivate weight/temperature obtained from the mass loss curves allowed us to determine the degradation temperatures of the different films.

Water sorption analysis

Water sorption isotherms were determined at 20°C by a gravimetric method with a Setaram (Caluire, France) B92 microbalance. The sample was introduced in the microbalance, and desorption *in vacuo* (2×10^{-6} mbar) was performed to determine the weight of the anhydrous sample. A partial pressure of water was established within the apparatus with an evaporator placed at considered temperature. The water uptake was followed as a function of time until equilibrium sorption was reached. The partial pressure was then increased in successive steps by changes in the temperature from −7 to 20°C, which allowed us to obtain the sorption isotherm. The equipment used was already presented in a previous article.[27]

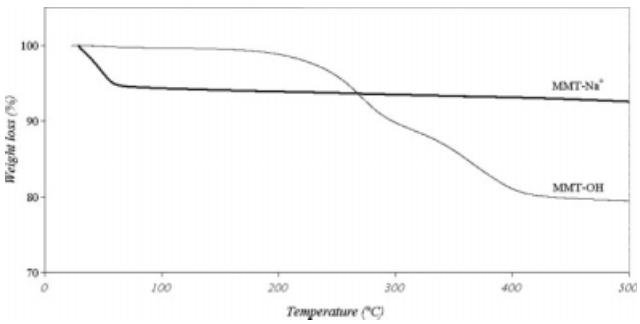

Figure 1 Thermogravimetric curves of the MMT-OH and MMT-Na^+ montmorillonites.

Oxygen permeability

Oxygen permeability measurements were performed at 20°C on a Mocon Oxtran (Minneapolis, MN) 2/21 equipped with a Coulox sensor. The test cell was composed of two chambers separated by the film (5 cm^2). Nitrogen, containing 2% hydrogen, was used as the carrier gas, and pure oxygen was used as the test gas. The relative humidity of the two gases was controlled by a humidifier and kept equal to 50 ± 3%. Before testing, specimens were conditioned in nitrogen/hydrogen inside the unit for at least 48 h to remove traces of atmospheric oxygen. The apparent oxygen transmission rate under N_2/H_2 was measured to give information on the background count due to leaks in the system. Subsequently, oxygen was introduced in the upstream compartment of the test cell. Oxygen transferred through the film was conducted by the carrier N_2/H_2 gas to the coulometric sensor. Measurements were made when the oxygen flux was stabilized, which indicated that the steady state was reached. The permeability coefficient [cm^3 (STP) μm/(m^2 day)] was calculated on the basis of oxygen transmission in the steady state, with the thickness of the films taken into account.

RESULTS AND DISCUSSION

TGA

Thermogravimetric weight loss curves of the nanoclays used in this study are shown in Figure 1. For each nanoclay, a first weight loss was observed between 30 and 115°C. This weight loss was attributed to a water

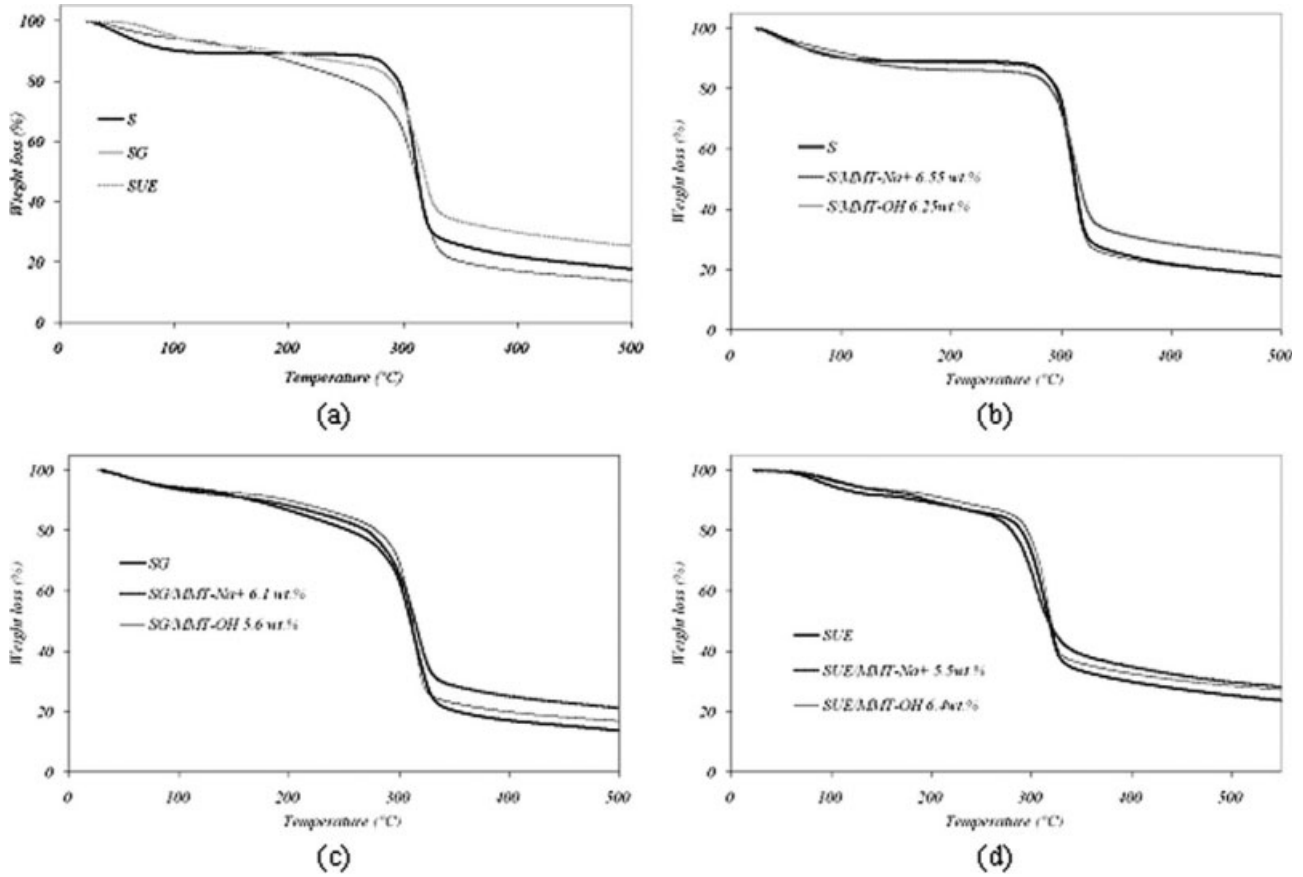

Figure 2 Thermogravimetric curves of the (a) starch, starch/glycerol, and starch/urea–ethanolamine films; (b) starch, starch/MMT-OH 6.25 wt %, and starch/MMT-Na^+ 6.55 wt % films; (c) starch, starch/glycerol/MMT-OH 5.6 wt %, and starch/glycerol/MMT-Na^+ 6.1 wt % films; and (d) starch/urea–ethanolamine, starch/urea–ethanolamine/MMT-OH 5.5 wt %, and starch/urea–ethanolamine/MMT-Na^+ 6.4 wt % films.

vaporization phenomenon. As shown, this water loss was important for MMT-Na^+ and much lower for MMT-OH, in agreement with a previous study[28] and the more hydrophobic surface of the organically modified clay. A second weight loss corresponding to the organic surfactant degradation was observed for MMT-OH. In fact, the organic fraction underwent degradation to volatiles in two steps between 115 and 500°C. The first organic fraction degradation, observed between 115 and 315°C, was due to the decomposition of the unconfined fraction of alkylammonium halide, consisting of the surfactant, which did not undergo the ion-exchange reaction inside the clay channel.[29–31] The second weight loss, observed between 315 and 500°C, was attributed to the thermal degradation of the other organic moieties. The total organic fraction was determined by the ratio of the total organic weight loss to the dry weight of montmorillonite. It is reported in Table I. As shown in Figure 1, the thermal stability of MMT-Na^+ was very important.

Thermogravimetric experimental results of the three reference matrices are presented in Figure 2(a). Two steps were observed on the weight loss curve relative to the starch film. The first step below 100°C corresponded to water loss, and the second one corresponded to starch decomposition at temperatures surrounding 313°C. The degradation mechanism consisted of the elimination of polyhydroxyl groups, accompanied by depolymerization and decomposition, with the final production of carbon.[32]

Three steps were evidenced on the weight loss curve of the starch-plasticized films. The first step corresponded to water loss. The second mass loss, between 100 and 250°C, was assigned to the volatization of water and plasticizers in agreement with Yang et al.'s[33] study. The last step corresponded to starch decomposition, with maximum decompositions at 315°C for the SG film and 318°C for the SUE film.

The thermogravimetric curves of the matrices and associated composites are compared in Figure 2(b,c,d) for S, SG, and SUE, respectively. From the values of the degradation temperatures deduced from the derivate weight/temperature, as reported in Table II, no significant difference, less than 3°C, was found in the thermal stability of the matrices after the incorporation of the nanoclays. The amount of inorganic phase in each composite was deduced from the weight residues measured at 450°C on the

TABLE II
Thermal Decomposition Temperatures of the Matrix and Composite Films and Nanoclay Content in the Composites Films

Sample	Maximum mass loss rate temperature (°C)	Experimental weight content of montmorillonite (inorganic + surfactant; wt %)[a]	Experimental volume inorganic content (vol %)[b]
Starch	313	—	—
S/MMT-OH	312	6.25	2.56
S/MMT-Na^+	314	6.55	3.71
SG	315	—	—
SG/MMT-OH	315	5.60	2.22
SG/MMT-Na^+	318	6.10	3.09
SUE	318	—	—
SUE/MMT-OH	317	5.50	2.16
SUE/MMT-Na^+	315	6.40	3.44

[a] Determined by TGA.
[b] Volume inorganic content determined with the density of each component of the composite.

nanocomposites and the respective matrices. As this inorganic phase was directly associated with the fillers, it was possible to calculate the experimental content of montmorillonite in each nanocomposite, with the weight fraction of surfactant in the nanoclay taken into account. The values are listed in Table II.

XRD and TEM analysis

XRD analysis was performed on native potato starch in a powder form and on the three different reference matrices. The results are presented in Figure 3(a). The diffraction diagram of the potato starch

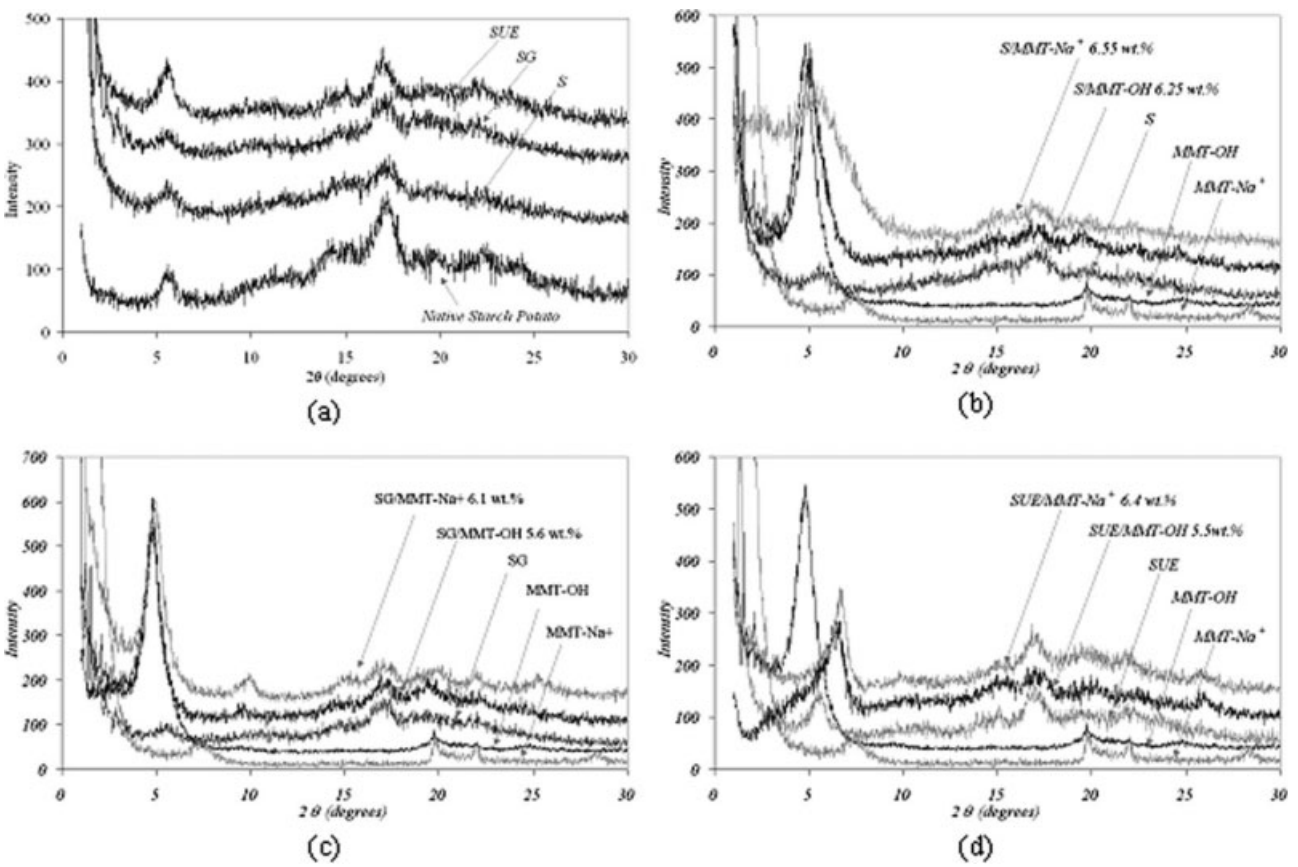

Figure 3 X-ray patterns of the (a) native starch potato in powder from, starch, starch/glycerol, and starch/urea–ethanolamine in film form; (b) MMT-OH and MMT-Na^+ powders, starch, starch/MMT-OH 6.25 wt %, and starch/MMT-Na+ 6.55 wt % films; (c) MMT-OH and MMT-Na^+ powders, starch/glycerol, starch/glycerol/MMT-OH 5.6 wt %, and starch/glycerol/MMT-Na+ 6.1 wt % films; and (d) MMT-OH and MMT-Na^+ powders, starch/urea–ethanolamine, starch/urea–ethanolamine/MMT-OH 5.5 wt %, and starch/urea–ethanolamine/MMT-Na^+ 6.4 wt % films.

powder corresponded to a typical XRD pattern of potato starch (B type).[34–36] The diffraction peaks observed for native potato starch at $2\theta = 5.6$, 11.4, 14.4, 17.1, 19.4, 22.3, and 24.3°, were related to complex structures, such as B-type crystals, characteristic of starch tubers.[37,38] The XRD patterns for all of the reference matrices films showed a decrease in the diffraction peak intensity compared to those of the native potato starch in powder form. These modifications were related to a decrease in the crystallinity due to the disorganization of starch molecules caused by heat treatment during the gelatinization process.[39] The presence of 20 wt % plasticizer in the system did not drastically modify the crystalline structure of the starch films.

After the incorporation of the nanoclays in the reference matrices, it was interesting to check, on one hand, the crystallinity of the matrix and, on the other hand, the state of dispersion of the fillers. The XRD patterns of the matrices and associated composites films are shown in Figure 3(b,c,d) for S, SG, and SUE, respectively. At high values of 2θ (from 10 to 30°), no noteworthy difference was observed after the incorporation of the nanoclays, whatever nanoclay and matrix were used. The crystallinity level remained then the same in the nanocomposites compared to the reference matrix.

We focused on the 2θ range between 1 and 10° to examine the dispersion state of the clays within the different matrices. Indeed, the XRD patterns of the two nanoclays in powder form presented in Figure 3(b,c,d) showed a low diffraction peak at $2\theta = 7.6°$ for MMT-Na^+, which corresponded to an interplatelet distance (d_{001}) equal to 11.7 Å, and a high diffraction peak at $2\theta = 4.8°$ for MMT-OH, which corresponded to a d_{001} value of 18.5 Å. This filler diffraction peak should, in theory, (1) be shifted to lower values of 2θ for intercalated clay structures within the matrix, (2) totally disappear for an exfoliated clay structure, and (3) stay at the same position in the case of microcomposite formation. However, we can remind one here that the characteristic peak of the B-type starch structure observed at $2\theta = 5.6°$ for all of the matrices should complicate the analysis of the clay dispersion state within the polymer phase. That is why TEM micrographs were also taken for the different nanocomposites.

We deduced from the analysis of the XRD patterns relative to the nanocomposite films that microcomposites were obtained when MMT-OH was introduced within the S and SG matrices, whereas intercalated structures were obtained for the same matrices with MMT-Na^+. These results were confirmed by the TEM micrographs of the different films. Indeed, according to the TEM images of the starch nanocomposites shown in Figure 4, MMT-Na^+ was found to disperse better in starch than

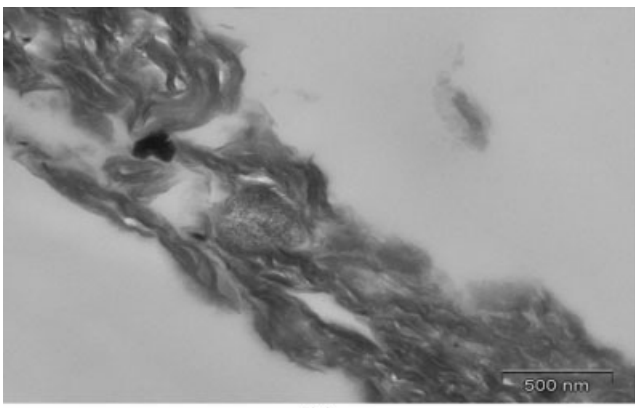

(a)

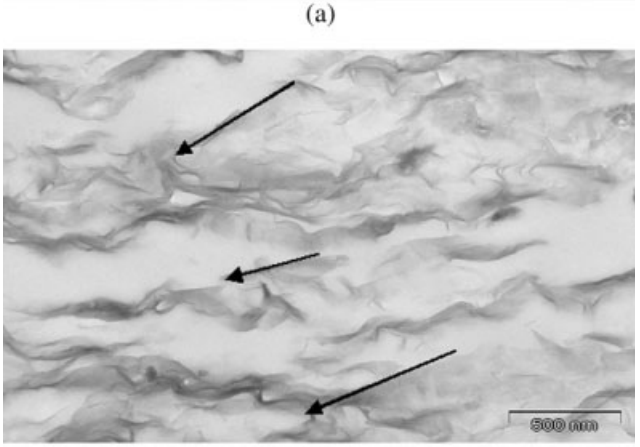

(b)

Figure 4 TEM micrographs of the (a) starch/MMT-OH 6.25 wt % film and (b) starch/MMT-Na^+ 6.55 wt % film.

MMT-OH. Dense stacks of MMT-OH layers were clearly observed, whereas much smaller aggregates were evidenced for MMT-Na^+. For the SG nanocomposites (Fig. 5), as in the case of pure starch nanocomposites, better dispersions were observed with MMT-Na^+ than with MMT-OH. Indeed, the silicate platelets were all in an aggregate form for MMT-OH, whereas a mix of different nanomorphologies (going from individual layers to some multilayers of intercalated silicate) was evidenced for MMT-Na^+.

A particularity was observed for the nanocomposites based on SUE as a matrix. Indeed, for these systems, a significant diffraction peak was observed at 6.8°, whatever nanoclay was used. For the nanocomposite film based on MMT-OH as a filler, an additional shoulder corresponding to pristine organoclay was observed at 4.8°. The diffraction peak centered at 6.8° could not be related to the nanoclay dispersion state, as this one appeared to be very different as a function of the clay from the TEM micrographs (Fig. 6). A better dispersion was indeed observed for MMT-Na^+ in comparison with MMT-OH in these systems. Further experiments are necessary to clearly explain this phenomenon, and they are underway.

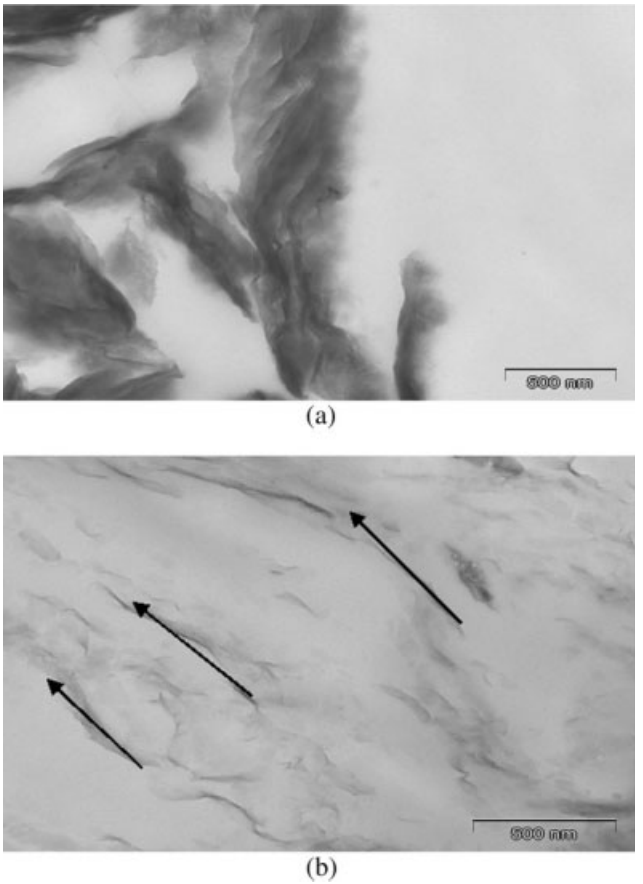

Figure 5 TEM micrographs of the (a) starch/glycerol/MMT-OH 5.6 wt % film and (b) starch/glycerol/MMT-Na^+ 6.1 wt % film.

For all nanocomposites reinforced by MMT-Na^+, TEM analyses showed an optimal orientation of silicate layers. Indeed, the silicate layers were parallel to the film surface, as shown by the arrows that were added on the TEM micrographs.

All of these morphological observations demonstrated that MMT-OH was less compatible with starch than MMT-Na^+. Indeed, despite the presence of hydroxyl groups in the interlayer gallery of MMT-OH, both XRD and TEM analyses showed a better dispersion of inorganic and hydrophilic MMT-Na^+ in the different matrices. The higher hydrophobic character of organoclays such as MMT-OH, which presents an advantage in comparison with the unmodified natural clays for a great majority of polymer matrices,[40,41] is a disadvantage for clay exfoliation in a highly polar and hydrophilic medium such as starch. As a result, MMT-OH did not disperse well; rather, it agglomerated and hardly formed a nanocomposite when introduced into starch. Furthermore, it was difficult to evidence from XRD and TEM analyses a significant role of the different plasticizers in the dispersion state of nanoclays. Indeed, whatever the matrix, the same kind of morphology was observed for a given clay. This was explained by the polar structure of the plasticizers that we used in this study.

Water sorption isotherm

The values of mass gain at equilibrium state for each water activity allowed us to plot the water sorption isotherm for each film. The sorption isotherms for native starch film and plasticized starch films are represented in Figure 7(a). The curves had a sigmoid shape, which corresponded to a type II classification of Brunauer, Emmett, and Teller among the five general types.[42] The Brunauer–Emmett–Teller II model, which is a combination of dual-mode (Langmuir sorption and Henry law) and Flory–Huggins contributions, is typical of water sorption in hydrophilic materials.[43] In the activity range $0 < a_w < 0.6$ (where a_w is the water activity), the amount of water sorbed at equilibrium was higher for native starch film compared to plasticized films. This could be related to a decrease of available sorption Langmuir's sites in the presence of a plasticizer. Indeed, the formation of thermoplastic starch was a result of strong interactions, hydrogen bonds, between the starch and

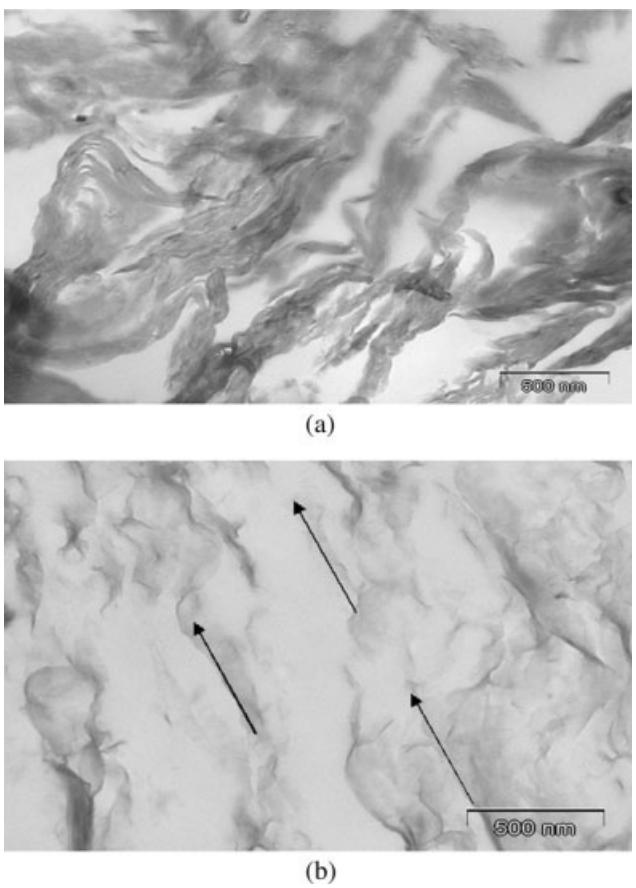

Figure 6 TEM micrographs of the (a) starch/urea–ethanolamine/MMT-OH 5.5 wt % film and (b) starch/urea–ethanolamine/MMT-Na^+ 6.4 wt % film.

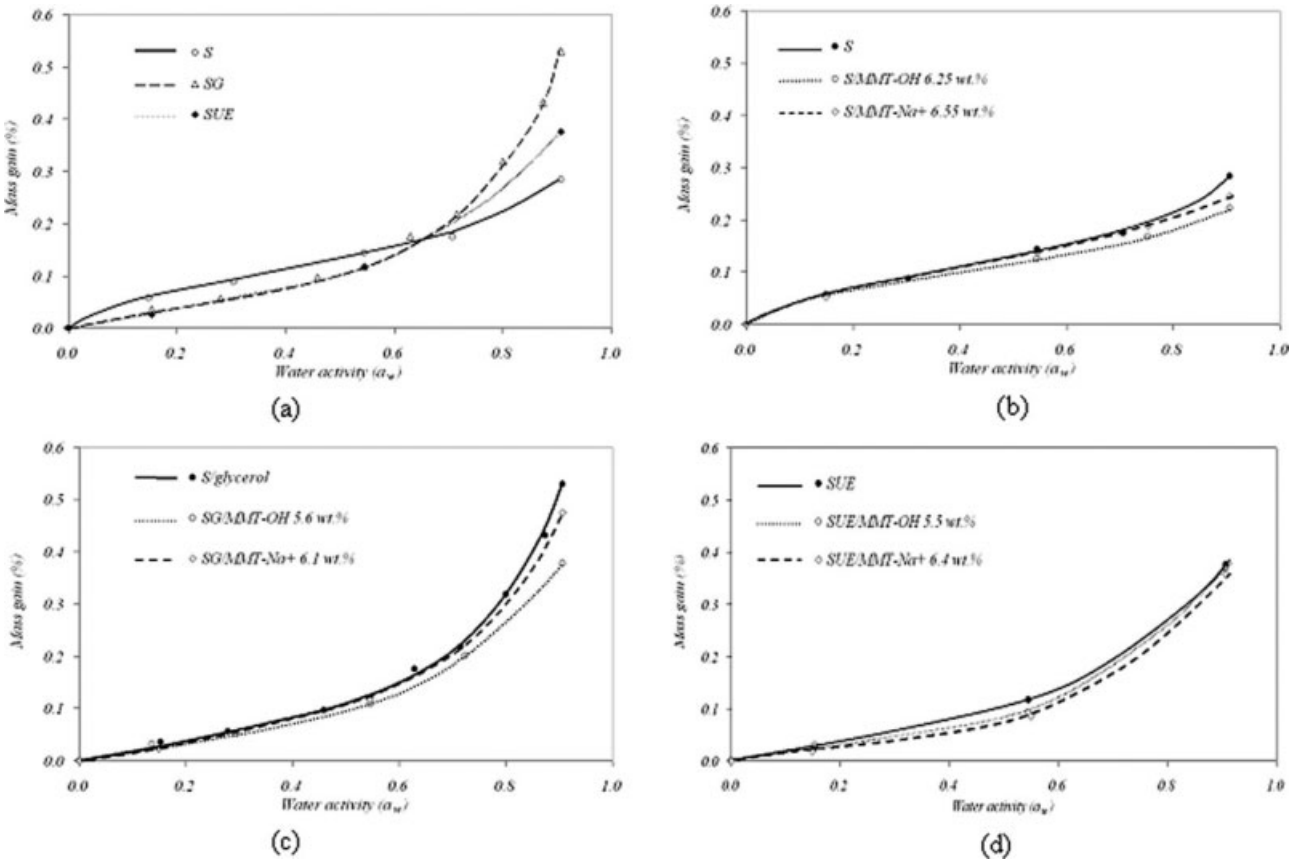

Figure 7 Water vapor isotherm at 20°C for the (a) starch, starch/glycerol, and starch/urea–ethanolamine films and MMT-Na^+ and MMT-OH powders; (b) starch, starch/MMT-OH 6.25 wt %, and starch/MMT-Na^+ 6.55 wt % films; (c) starch, starch/glycerol/MMT-OH 5.6 wt %, and starch/glycerol/MMT-Na^+ 6.1 wt % films; and (d) starch/urea–ethanolamine, starch/urea–ethanolamine/MMT-OH 5.5 wt %, and starch/urea–ethanolamine/MMT-Na^+ 6.4 wt % films.

plasticizers. OH groups in ethanolamine, O=C and NH_2 groups in urea, and OH groups in glycerol could form hydrogen bonds with the OH groups of the starch, which led to a decrease in the concentration of polar available sites in the plasticized films.[25,44,45] In the activity range $0.6 < a_w < 0.9$, an increase of water sorption was observed for each sample, and it could be related to a water-clustering phenomenon. This phenomenon was favored in the plasticized films because of the enhanced molecular mobility of the polymer chains in the presence of plasticizer, on one hand, and to the hydrophilicity of the plasticizer, on the other hand.[45–47] Indeed, the water uptake at high activities was higher for plasticized films than for native starch film. Furthermore, compared to the urea–ethanolamine mixture, glycerol had a more hydrophilic character and contributed to higher water swelling at high a_w values.

The water sorption isotherms of the reference matrices were fit to the Guggenheim–Anderson–de Böer (GAB) equation, which has been shown to describe appropriately the water sorption isotherms of many cellulosic materials[48] and hydrophilic biopolymers[27,49] over a range of a_w up to 0.9:[25]

$$M = M_m \frac{C_G K a_w}{(1 - K a_w)(1 + (C_G - 1) K a_w)} \quad (1)$$

where M is the equilibrium moisture content of the films on a dry basis, M_m is the monolayer moisture content and represents the water content corresponding to the saturation of all primary absorption sites by one water molecule, C_G is the Guggenheim constant and represents the energy associated with the binding between the water molecules and primary interactions sites or monolayer, and K is a factor correcting properties of the multilayer molecules with respect to the bulk liquid.

To evaluate the accuracy of the GAB model to describe the experimental water sorption isotherms of our different films, the mean relative percentage deviation modulus (E) was used. It is defined by

$$E = \frac{100}{N} \sum_{i=1}^{N} \frac{|m_i - m_{pi}|}{m_i} \quad (2)$$

where m_i is the experimental value, m_{pi} is the predicted value, and N is the number of experimental

TABLE III
GAB's Model Constants (M_m, C_G, and K), E Values, and MCS Values Estimated at 50% Relative Humidity for the S, SG, and SUE Films

Film	M_m	C_G	K	E (%)	MCS
S	0.090	10.200	0.765	2.4	0.60
SG	0.073	3.713	0.961	4.3	1.03
SUE	0.075	3.431	0.897	7.5	1.00

data. E is widely adopted through the literature, and a modulus value below 10% indicates a good fit for practical purposes.[50]

We calculated the constants M_m, C_G, and k by fitting according to the software Tablecurve 2D (Jandel Scientific, San Rafael, CA). Table III shows the values of the constants and the associated E (%) values for the three reference matrices. The values of E were inferior to 10%, which thus showed accurate fits. Examination of the GAB parameters showed that the values of M_m were lower in the presence of plasticizers. This was due to the decreasing availability of active sites for water binding to form the monolayer.[51] Moreover, the value of M_m was relatively similar, whatever the plasticizers, glycerol or urea/ethanolamine. C_G was also lower in the presence of plasticizers. This was indicative of a decrease in binding energy for the first sorbed water layer in the presence of plasticizers. The decrease of C_G was associated with an increasingly shorter residence time for the water molecules sorbed in the first layer. Finally, the increase in K values observed on the plasticized reference films indicated a reduction in sorption energy in the absolute value of the multilayers. This effect was particularly emphasized for the SG film, which had the higher swelling capability.

The range of a_w, in which the self-association of water molecules occurred, could be determined by application of the clustering function. Zimm and Lundberg[52,53] developed a method that analyzes water clustering from the single shape of the experimental isotherm. They developed, on the bases of statistical mechanics, a method that gives an interpretation of the solution thermodynamic behavior from the shape of the isotherm. The relation appears as follows:

$$\frac{G_S}{V_S} = -(1-\Phi_S)\left[\frac{\partial(a_w/\Phi_S)}{\partial a_w}\right]_{p,T} - 1 \qquad (3)$$

where G_S is the cluster integral, V_S is the partial molecular volume of the water molecules, at constant pressure p and temperature T. Φ_S is the volume fraction of the water molecules in film.

A G_S/V_S value equal to -1 indicates that solvent dissolves into the polymer matrix randomly; instead, higher values, $G_S/V_S > -1$, mean that the concentration of water in the neighborhood of a given water molecule is greater than the average concentration of water molecules in the polymer. The quantity $G_S\Phi_S/V_S$ is the mean number of molecules in excess of the mean concentration of penetrant in the neighborhood of a given water molecule.[54,55]

Thus, the mean cluster size (MCS) can be evaluated by

$$\mathrm{MCS} = 1 + \left(\frac{\Phi_S G_S}{V_S}\right) \qquad (4)$$

With the GAB model parameters, M_m, C_G, and K, MCS can be expressed as follows:[45]

$$\mathrm{MCS} = \frac{(\rho_s/\rho_p)^2}{M^2(1+(\rho_s/\rho_p)/M)^2} \times \left[1 - \frac{M}{M_m C_G}(-2Ka_w(C_G-1) - 2 + C_G)\right] \qquad (5)$$

where ρ_s and ρ_p are the densities of the water molecules and polymer, respectively.

The plots of MCS versus activity for the different reference films are presented in Figure 8. The onset of water autoassociation in the unplasticized starch film was observed to occur at $a_w = 0.79$. The addition of plasticizers favored water molecule clustering at lower a_w values (0.48 for both plasticizers, glycerol and urea/ethanolamine). This was due to a decrease in available sorption sites (polar groups of starch) in the presence of plasticizer and to an increase in the polymer chain mobility in these systems. The MCS values obtained at $a_w = 0.5$ are listed in Table III. In this standard use condition, MCS was approximately the same for the two plasticized starch films (1.03 for SG and 1.00 for SUE). The MCS value was lower for unplasticized starch (0.60).

The sorption isotherms for matrices and associated composites are represented in Figure 7(b,c,d) for

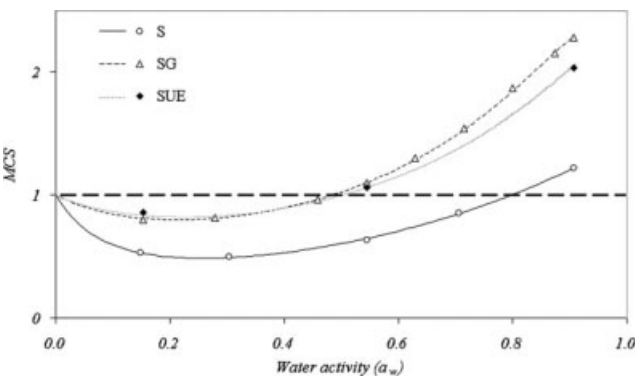

Figure 8 Evolution of MCS calculated from GAB's equation versus a_w for the starch, starch/glycerol, and starch/urea–ethanolamine films.

native S, SG, and SUE, respectively. The shape of the curve was similar for all of the samples, which indicated that no major modifications of the sorption mechanism occurred in the nanocomposites in comparison with the reference matrix films. For starch and starch/glycerol reinforced by MMT-OH [Fig. 7(b,c)], a small decrease in water sorption was observed compared to the reference matrices. As shown in Figure 7(a), MMT-OH was much less hydrophilic than the reference matrices. Therefore, the participation of MMT-OH in the sorption process was very insignificant compared with the hydrophilic matrix. MMT-OH could then be considered an impermeable filler dispersed within the polymer matrix for water sorption. For composites based on MMT-Na^+, the situation was not exactly the same. Indeed, the water sorption ability of the nanocomposite and the respective matrix (S or SG) was nearly identical in the entire activity range. This result can be explained by the hydrophilic character of MMT-Na^+ due to the presence of the Na^+ cation. This montmorillonite, whose water adsorption capacity was high [Fig. 7(a)], was then able to participate in the general moisture sorption process of the nanocomposite.[28]

The isotherm curves for starch/urea–ethanolamine and the associated composites reinforced by MMT-Na^+ and MMT-OH are shown in Figure 7(d). A decrease in water uptake was observed for all of the composites with respect to the reference matrix, independently of the nature of the nanoclay. From this observation, it seems that the microstructure changes evidenced by XRD analysis after the addition of nanoclay could play a role in the sorption mechanism. In particular, the suspected ordered phase implied that the nanoclays and the plasticizers could mask the initial hydrophilicity of MMT-Na^+.

From all these results, we concluded that the water uptake in the nanocomposite films depended mainly on the water uptake capacity of each component or phase in the system. If the water uptake variation observed after clay insertion remained quite low (few percentages), the trends that were observed, that is, similar or decreased values of the water uptake in the composite material with respect to the respective matrix, were not detrimental to the barrier properties.

Oxygen permeability

Oxygen permeability measurements were performed at 50% relative humidity, which is a standard use condition. The results obtained for all systems are shown in Figure 9. The oxygen permeability of both plasticized starch films was higher compared to the native starch film. This was explained by the greater flexibility of the polymer chains in the presence of plasticizer and also to the beginning of the water-clustering phenomenon at this activity for the plasticized starch films, contrary to the neat starch film.

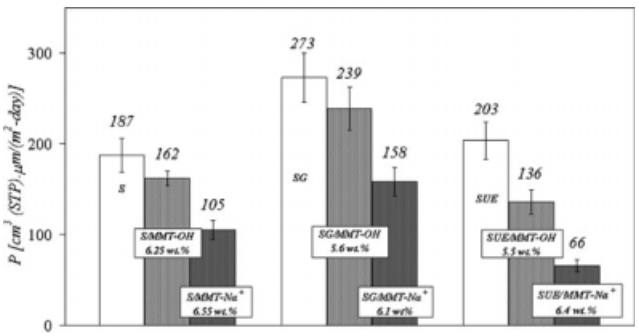

Figure 9 Oxygen permeability coefficients of the S, SG, and SUE matrices and associated composites.

As shown in Figure 9, the addition of nanoclay, either MMT-OH or MMT-Na^+, within the matrices decreased the oxygen permeability. The layered silicate could be viewed as an impermeable obstacle to the motion of oxygen molecules and could then greatly affect the gas transport properties. Whatever the matrix, the reduction of oxygen permeability was more important after the insertion of MMT-Na^+. For example, for the starch system, reductions in the oxygen permeability of 14 and 44% were observed in the presence of MMT-OH and MMT-$Na^{+,}$ respectively. We previously evidenced that, under conditions of the oxygen permeability measurements (50% relative humidity), the water content was slightly higher for the nanocomposite based on MMT-Na^+ than for the nanocomposite based on MMT-OH. The difference observed in the magnitude of gas permeability reduction as a function of the clay nature was then essentially due to the state of dispersion of the nanoclay in the matrix. As shown by the XRD and TEM analysis, the dispersion state was better for MMT-Na^+ compared to MMT-OH, which led to a higher tortuosity effect.

Nielsen[56] derived a simple model strictly based on a tortuosity point of view to describe the permeability in silicates nanocomposites. The model supposes that each layer is oriented perpendicularly to the diffusion pathway of the gas. The presence of impermeable nanoclay introduces a tortuous pathway for the diffusing oxygen molecules. The reduction of permeability initiates from the longer diffusive path that the oxygen molecules must travel in the presence of the layered silicates. It is possible to define a tortuosity factor (τ) as the ratio of the distance (d') that oxygen molecules must travel in the presence of the layered silicates and the distance (d) that they would travel in the absence of layered silicates. The

TABLE IV
Water Vapor Sorption Properties and Oxygen Transport Properties of the Different Matrix and Nanocomposite Films

Sample	M (%)	P	$P_{composite}/P_{matrix}$	τ
S	13.3	187	—	—
S/MMT-OH 6.25 wt %	11.9	162	0.87	1.12
S/MMT-Na^+ 6.55 wt %	12.9	105	0.56	1.71
SG	10.8	273	—	—
SG/MMT-OH 5.6 wt %	9.8	239	0.88	1.12
SG/MMT-Na^+ 6.1 wt %	10.1	158	0.58	1.67
SUE	10.3	203	—	—
SUE/MMT-OH 5.5 wt %	8.2	136	0.67	1.47
SUE/MMT-Na^+ 6.4 wt %	7.4	66	0.32	3.00

M = equilibrium water content of the films on a dry basis; P = oxygen permeability coefficient measured [cm^3 (STP) $\mu m/(m^2$ day)] at 20°C and 50% relative humidity; $P_{composite}/P_{matrix}$ = relative permeability; τ = tortuosity value deduced from Nielsen law.

effect of tortuosity on the permeability can be expressed as follows:

$$\frac{P_{composite}}{P_{matrix}} = \frac{1 - \phi_S}{\tau} \quad (6)$$

where $P_{composite}$ and P_{matrix} are the permeability coefficients of the composite and pure matrix, respectively, and ϕ_s is the volume fraction of the inorganic layered nanoclays.

The values of τ were calculated for all of the composites from the ratio of each nanocomposite permeability to that of the respective matrix. The τ values are listed in Table IV. For each system, a higher tortuosity value was obtained for composites reinforced by MMT-Na^+ compared to those reinforced by MMT-OH (e.g., $\tau = 1.11$ for S/MMT-OH and $\tau = 1.72$ for S/MMT-Na^+). These results are in a good agreement with the state of dispersion determined from XRD and TEM analyses. The same tortuosity values were obtained for the nanocomposites based on the glycerol-plasticized starch with respect to the SG matrix ($\tau = 1.12$ for S/G/MMT-OH and $\tau = 1.67$ S/G/MMT-Na^+). We then concluded that the introduction of nanoclay played the same role in the S and SG matrices. This result was in agreement with previous conclusion obtained from morphological analysis. Indeed, the clay dispersion state did not depend on the presence of glycerol within the matrix, and clay introduction did not modify the matrix crystalline morphology for either the starch or starch/glycerol matrix. However, higher tortuosity effects were observed in the nanocomposites based on the starch/urea–ethanolamine matrix. τ was equal to 1.47 in the case of MMT-OH, and it reached a value of 3.0 in the case of MMT-Na^+. TEM images showed that the state of dispersion of the nanoclay was very similar whatever the plasticizer used, so the additional increase of tortuosity was due to the particular ordered phase, which implied nanoclays and urea–ethanolamine, which was evidenced by XRD analysis in these systems.

CONCLUSIONS

New environmentally friendly composites were prepared via a solution/casting method from a natural potato starch matrix and lamellar nanofillers. Two nanoclays, a natural montmorillonite modified with methyl tallow bis-2-hydroxyethyl quaternary ammonium and a natural purified montmorillonite, were chosen. The influence of the addition of a plasticizer in the formulation was also studied, and two compatibilizers were chosen, glycerol and a 50/50 mixture of urea–ethanolamine.

The TGA curves showed no significant difference in the thermal stabilities of the matrices after the incorporation of the nanoclays.

Whatever the matrices, both the XRD and TEM results evidenced an improved dispersion state for MMT-Na^+ in comparison with MMT-OH. The hydrophilic character of the pristine clay promoted the formation of favorable interactions between the clay gallery and the hydroxyl groups of starch, which led to a mixture of exfoliated and intercalated structures lying parallel to the film surface. On the contrary, microcomposites were systematically obtained from the formulations based on the organomodified MMT-OH clay. The clay dispersion state was not significantly influenced by the addition of a plasticizer to the matrix, as it did not drastically modify the polarity of the medium.

No significant modification of the matrix crystalline structure was observed after clay addition for the starch and starch–glycerol matrices. A particularity was, however, observed for the nanocomposites based on starch/urea–ethanolamine. Indeed, for these systems, a significant diffraction peak was observed at 6.8°, whatever the nanoclay used. The development of a particular ordered phase, which implied the nanoclays and the compatibilizers, was then suspected to occur for these materials.

The water uptake in the nanocomposite films did not depend on the state of dispersion of the nanoclays. It was principally related to the water uptake capacity of each component or phase in the system. A decrease in water sorption was then observed for the nanocomposites reinforced by the low hydrophilic MMT-OH in comparison with the reference matrices. On the contrary, because of its initial hydrophilic character, MMT-Na^+ was able to participate in the general moisture sorption process for starch and starch/glycerol based materials. As a

result, low differences were observed between the water uptakes of the nanocomposites based on this clay and the respective matrices. A specific behavior was evidenced for the nanocomposites obtained from MMT-Na^+ and starch/urea–ethanolamine. It seemed that the microstructure changes evidenced by XRD analysis after the addition of nanoclay played a role in the sorption mechanism. In particular, the suspected ordered phase, which implied the nanoclays and the plasticizer, seemed to mask the initial hydrophilicity of MMT-Na^+. A decrease in the water uptakes was then observed with the addition of pristine clay within this matrix, and this decrease was similar to that observed with MMT-OH. The general effect of the plasticizers (glycerol or urea–ethanolamine) was also studied on the water sorption mechanism. The main role of this additional component was to decrease the water uptake at low activity and to favor water swelling at high activity. In particular, a water-clustering phenomenon began at lower activity for the plasticized films in comparison with the unplasticized ones.

The oxygen permeability coefficient was determined at 50% relative humidity for the different films. The permeability coefficients of all of the plasticized starch films were higher than those measured for the native starch film. This trend was related to the increase in the polymer chain mobility in the presence of plasticizers. Whatever the matrix, a general decrease in the oxygen permeability was observed with the addition of the nanoclays. The fillers could be considered as impermeable to the motion of oxygen molecules, and the permeability decrease was more pronounced with MMT-Na^+ because of a better dispersion state. Among all of the nanocomposite films, the most promising material was obtained from starch, urea–ethanolamine, and MMT-Na^+ because of a lower water uptake and higher gas barrier properties. These final properties resulted, of course, from a high dispersion state of the nanoclays within the matrix but also from specific interactions between urea–ethanolamine and the nanoclays. These interactions seemed to lead to the formation of an additional ordered phase in the material, which appeared to bring a significant contribution to both water and gas barrier property improvement. Further work will deal with the characterization of this phase and also enlarge our studies to a wider range of nanoclay contents and other processing modes.

The authors gratefully acknowledge Pierre Alcouffe and the Centre Technologique des Microstructures of University of Lyon 1 for TEM photomicrographs and Ruben Vera and the Centre de Diffractométrie Henri Longchambon of University of Lyon 1 for XRD analysis.

References

1. Petersson, L.; Oksman, K. Compos Sci Technol 2006, 66, 2187.
2. Hartman, J.; Albertsson, A. C.; Lindblad, M. J Appl Polym Sci 2006, 100, 2985.
3. Xu, Y.; Ren, X.; Hanna, M. A. J Appl Polym Sci 2006, 99, 1684.
4. Avella, M.; De Vlieger, J.; Errico, M. Food Chem 2005, 93, 467.
5. Chen, B.; Evans, J. R. G. Carbohydr Polym 2005, 61, 455.
6. Dole, P.; Joly, C.; Espuche, E. Carbohydr Polym 2004, 58, 335.
7. Mali, S.; Grossmann, M.; Garcia, M. Carbohydr Polym 2002, 50, 379.
8. Arvanitoyannis, I.; Biliaderis, C. Food Chem 1998, 3, 333.
9. Chen, M.; Chen, B.; Evans, R. G. Nanotechnology 2005, 16, 2334.
10. Yilmaz, G.; Jongboom, R.; Feil, H. Biomacromolecules 2004, 5, 650.
11. Ma, X.; Yu, J.; Wang, N. Macromol Mater Eng 2007, 292, 723.
12. McGlashan, S.; Halley, P. Polym Int 2003, 52, 1767.
13. Picard, E.; Vermogen, A.; Gerard, J. F.; Espuche, E. J Membr Sci 2007, 292, 133.
14. Vlasveld, D. P. N.; Groenewold, J.; Bersee, H. E. N. Polymer 2005, 46, 12567.
15. Messersmith, P. B.; Giannelis, E. P. Chem Mater 1994, 6, 1719.
16. Messersmith, P. B.; Giannelis, E. P. J Polym Sci Part A: Polym Chem 1995, 33, 1047.
17. Vaia, R. A.; Giannelis, E. P. Macromolecules 1997, 30, 8000.
18. Lepoittevin, B.; Devalckenaere, M.; Pantoustier, N.; Alexandre, M. Polymer 2002, 43, 4017.
19. Hotta, S.; Paul, D. R. Polymer 2004, 45, 7639.
20. Gain, O.; Espuche, E.; Pollet, E. J Polym Sci Part B: Polym Phys 2005, 43, 205.
21. Huang, M.; Yu, J. J Appl Polym Sci 2005, 99, 170.
22. Huang, M.; Yu, J.; Ma, X. Carbohydr Polym 2006, 63, 393.
23. Kampeerapappun, P.; Aht-Ong, D.; Pentrakoon, D. Carbohydr Polym 2007, 67, 155.
24. Pereda, M.; Aranguren, M.; Marcovich, N. J Appl Polym Sci 2008, 107, 1080.
25. Talja, R. A.; Helen, H.; Ross, Y. H. Carbohydr Polym 2007, 67, 288.
26. Ma, X.; Yu, J. Carbohydr Polym 2004, 57, 197.
27. Despond, S.; Espuche, E.; Domard, A. J Polym Sci Part B: Polym Phys 2001, 39, 3114.
28. Picard, E.; Gauthier, H.; Gerard, J. F. J Colloid Interface Sci 2007, 307, 364.
29. Cervantes, J.; Cauih-Rodriquez, J.; Varquez-Torre, H. Thermochim Acta 2007, 457, 92.
30. Edwards, G.; Halley, P.; Kerven, G. Thermochim Acta 2005, 429, 13.
31. Monticelli, O.; Musina, Z.; Frache, A. Polym Degrad Stab 2007, 92, 370.
32. Cyras, V.; Zenklusen, M.; Vazquez, A. J Appl Polym Sci 2006, 101, 4313.
33. Yang, J.; Yu, J.; Ma, J. Carbohydr Polym 2006, 66, 110.
34. Krogas, K.; Heinamaki, J.; Karjalainen, M. Int J Pharm 2003, 251, 205.
35. Lim, S. T.; Chang, E. H.; Chung, H. J. Carbohydr Polym 2001, 46, 107.
36. Zobel, H. F. Starch 1998, 40, 44.
37. Cheetham, N.; Tao, L. Carbohydr Polym 1998, 36, 277.
38. Mali, S.; Grossmann, M.; Garcia, M. Carbohydr Polym 2002, 50, 379.
39. Cooke, D.; Gidley, M. J. Carbohydr Res 1992, 227, 103.
40. Dean, K.; Yu, L.; Wu, D. Y. Compos Sci Technol 2007, 67, 413.
41. Park, H.; Lee, W. K.; Park, C. Y. J Mater Sci 2003, 38, 909.
42. Brunauer, S.; Deming, L. S.; Teller, E. J Am Chem Soc 1940, 62, 1723.
43. Rahman, S. Food Properties Handbook; CRC: Boca Raton, FL, 1995.
44. Ma, X.; Yu, J. Carbohydr Polym 2006, 64, 267.

45. Mali, S.; Sakanaka, F.; Yamashita, F. Carbohydr Polym 2005, 60, 283.
46. Godbillot, L.; Dole, P.; Joly, C.; Roge, B.; Mathlouthi, M. Food Chem 2006, 96, 380.
47. Enrione, J. I.; Hill, S. E.; Mitchell, J. R. J Agric Food Chem 2007, 55, 2956.
48. Gouanve, F.; Marais, S.; Bessadok, A. J Appl Polym Sci 2006, 101, 4281.
49. Despond, S.; Espuche, E.; Cartier, N. J Polym Sci Part B: Polym Phys 2005, 43, 48.
50. Basu, S.; Shivhare, U. S. Dry Technol 2006, 24, 917.
51. Muhtaseb, A. H.; McMinn, W. A. M.; Magee, T. R. A. J Food Eng 2004, 61, 297.
52. Lundberg, J. L. Pure Appl Chem 1972, 31, 261.
53. Zimmn, B. H.; Lundberg, J. L. J Phys Chem 1956, 60, 425.
54. Aranda, P.; Wen-Janq, C.; Martin, C. R. J Membr Sci 1995, 99, 185.
55. Del Nobile, M. A.; Mensitieri, G.; Sommazzi, A. Polymer 1995, 36, 4943.
56. Nielsen, E. J Macromol Sci Chem 1967, A1, 929.